5-7-2021

# Centralized Thermal Stress Oriented Dispatch Strategy for Paralleled Grid-Connected Inverters Considering Mission Profiles

Luocheng Wang
*University of North Carolina at Charlotte*

Tiefu Zhao
*University of North Carolina at Charlotte*

Jiangbiao He
*University of Kentucky*, Jiangbiao.He@uky.edu

# Centralized Thermal Stress Oriented Dispatch Strategy for Paralleled Grid-Connected Inverters Considering Mission Profiles

Digital Object Identifier (DOI)
https://doi.org/10.1109/OJPEL.2021.3078416

Notes/Citation Information
Published in *IEEE Open Journal of Power Electronics*, v. 2.

IEEE Open Journal of
Power Electronics

Received 21 March 2021; revised 28 April 2021; accepted 2 May 2021. Date of publication 7 May 2021;
date of current version 24 May 2021. The review of this article was arranged by Associate Editor
Ui-Min Choi.

*Digital Object Identifier 10.1109/OJPEL.2021.3078416*

# Centralized Thermal Stress Oriented Dispatch Strategy for Paralleled Grid-Connected Inverters Considering Mission Profiles

**LUOCHENG WANG [1] (Student Member, IEEE), TIEFU ZHAO [1] (Senior Member, IEEE), AND JIANGBIAO HE [2] (Senior Member, IEEE)**

[1] Electrical and Computer Engineering Department, University of North Carolina at Charlotte, Charlotte, NC 28223 USA
[2] Electrical and Computer Engineering Department, University of Kentucky, Lexington, KY 40506 USA

CORRESPONDING AUTHOR: LUOCHENG WANG (e-mail: lwang45@uncc.edu).

This work was supported by the North Carolina Renewable Ocean Energy Program, administered by the Coastal Studies Institute.

**ABSTRACT** One of the major failure causes in the power modules comes from the severe thermal stress in power semiconductor devices. Recently, some local control level methods have been developed to balance the power loss, dealing with the harsh mission profile, in order to reduce the thermal stress. However, there is not any specific system level strategy to leverage these local control level methods responding to the multiple inverters situation. Besides, the impacts of these methods on the thermal cycle and lifetime of the power modules in the long-term time scale have not been evaluated and compared yet. Hence, in this article, a centralized thermal stress oriented dispatch (TSOD) strategy is proposed to take full advantage of these local control level methods, including the switching frequency variation and the reactive power injection, to reduce the thermal stresses for multiple inverters. In addition to the PI controller, the finite control set model predictive control (FCS-MPC) is also explored to synergize with the proposed strategy. The results from the real-time model-in-the-loop testing on a four-paralleled-inverters platform, the reliability assessment, and the experiments all validate the effectiveness of the proposed centralized TSOD strategy on the thermal stress reduction.

**INDEX TERMS** Centralized method, converter control, finite control set model predictive control, mission profile, reactive power injection, reliability assessment, switching frequency variation, thermal stress.

## I. INTRODUCTION

Grid-connected inverters are playing a significant role in the distributed energy resource (DER) systems to transmit and synchronize the power from the renewable energy mechanism, such as the wind turbine or the solar panel, to the main utility grid. In the most widely used inline configuration, the grid-connected inverter connects the DC link and the AC grid. The main function is to regulate the DC link voltage and transmit the real power [1]. Meanwhile, the current industrial inverter unit is also equipped with other functions, such as the reactive power control, which provides this inline configuration with more flexibilities in practical applications.

However, the lifetime of the grid-connected inverter in this configuration extremely suffers from the intermittent renewable energy generation. The generated power or the mission profile usually has a large variation in a short duration [2]–[5]. Due to the inline structure, the grid-connected inverter will bear such a variation of the real power from hundreds of kilowatts to several megawatts. Subsequently, a fast-varying power loss is aggregated, and a severe thermal cycling occurs in the power module of the converter. Both the bond-wire liftoff and the solder joint fatigue, two most frequent failure modes of the power module, have been justified related to this thermal stress. Thus, the thermal stress reduction, which is oriented to reduce the temperature swing and mean values, is always critical to extend the device lifetime online and improve the system reliability [6].

In the purpose of relieving such a thermal stress, several researches have been carried out on the local control level [7]–[21]. Based on the different concentrations, most of them can

be divided into the modulation strategy and the control target strategy. In the modulation strategy, the main approach is to change the switching frequency of the pulse width modulation (PWM) [8]–[12]. Because the switching loss takes up a significant portion of the power loss in high power applications, the change of the switching frequency would explicitly level the power loss over the varying mission profile and further reduce the thermal stress. The initial concept is presented in [8], where the range of the junction temperature is partitioned into different zones and the switching frequency is adjusted to confine the junction temperature in the moderate zone. An improved method is proposed in [9] by using the state machine to identify operating states of semiconductor devices and adjust the switching frequency. A combined modulation method is presented in [11] and [12], that the discontinuous-PWM and continuous-PWM are adopted respectively for the high power and the low power loadings, where the switching frequency decreases by discontinuous-PWM in the high power period and so does the switching loss. In general, the switching frequency variation is the main methodology in this strategy, which helps to level the power loss over the mission profile and reduce the thermal stress. However, the local controller complexity has been much increased and may adversely affect the stability of the system.

The second one is the control target strategy. The main approach is to change the operating point of the power converter [13]–[18]. This is attributed to the dependency of the power loss on the conduction current and the device voltage. One control target is the DC link voltage [13], [14], where the link voltage is adapted during the low speed operation of the motor drive to reduce the semiconductor device voltage and so does the switching loss. However, the DC link voltage adaption sacrifices the output voltage limit of all linked converters and may deteriorate the thermal stress on other linked power converters. Another control target is the reactive power [15]–[18]. The reactive power directly changes the conduction current flowing through the power converter, which would adjust both the conduction loss and the switching loss of power modules. Superior to the DC link voltage adaption, the reactive power injected to one converter is isolated from others. This method is investigated between paralleled neutral point clamped (NPC) converters in [15], [16]. In addition to the capability of the low-voltage ride through (LVRT), it has been validated that the reactive power can reduce the thermal stress by injecting either a capacitive or an inductive value, which is also justified for the shunt configuration in DER systems [17]. However, this reactive power injection method can only generate more power losses than the one under the unity power factor control, which means it would reduce the temperature swing value, but increase the mean value in return. Hence, the impact of the reactive power injection on the lifetime and the reliability becomes ambiguous.

Besides, some novel converter controllers are also noticed to have the potential to reduce the thermal stress of inverters, such as the finite control set model predictive control (FCS-MPC) [19], [20]. Due to the switching frequency variation property of the FCS-MPC [21], the switching frequency and the conduction current can be adjusted simultaneously by only injecting the reactive power to the FCS-MPC controlled power converters. Accordingly, the power loss is balanced, and the thermal stress would be effectively reduced.

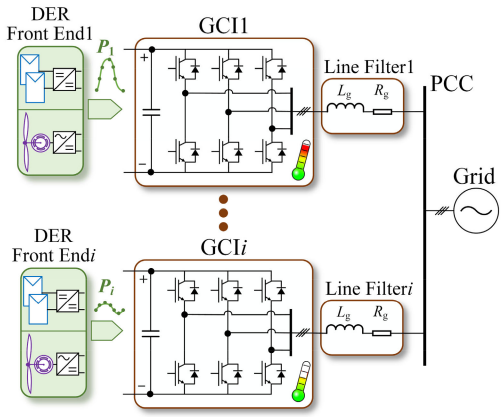


**FIGURE 1.** System diagram of multiple inverters based DER system.

However, most of the existing methods focused locally and have not been tested in the multiple DER systems. Their performances on the thermal stress reduction have not been qualitatively compared. Besides, for those requiring the coordination between paralleled converters, such as the reactive power injection, there is not any specific system level strategy to leverage those local thermal stress reduction methods. More importantly, their impacts on the lifetime of power modules and the reliability of DER systems in the long-term time scale have not been evaluated. Therefore, in this paper, a system-level centralized thermal stress oriented dispatch strategy is proposed for multiple DER systems, which reduces the thermal stresses of paralleled grid-connected inverters. It takes effect by inspecting the real-time junction temperature, the operating state and the health condition of each inverter. The switching frequency variation and the reactive power injection are imported separately to this strategy, combining with either conventional PI or FCS-MPC local controller, in order to compare their performances on the thermal stress reduction. Eventually, their impacts on the thermal cycles and the lifetime of power modules will be investigated.

The rest content of this paper is organized as follows: the proposed centralized thermal stress oriented dispatch strategy is introduced in Section II. The real-time simulation verification is presented in Section III through a four-paralleled-grid-connected-inverters system. The reliability assessment and tradeoff analysis are given in Section IV. Experimental results are shown in Section V from a digital twin hardware platform and conclusions come to the last.

## II. PROPOSED CENTRALIZED THERMAL STRESS ORIENTED DISPATCH STRATEGY

Fig. 1 shows a typical system diagram of the multiple inverters based DER system which consists of paralleled two-level

three phases grid-connected inverters (GCIs). These GCIs experience different mission profiles and suffer from different severities of the thermal stress. The thermal profile, including the junction $T_j$, the case $T_c$, and the heatsink $T_h$ temperatures of the power module, is normally determined by the power loss of the power converter, the designed thermal management system and the ambient temperature $T_a$. Conventionally, the power loss is the only degree of freedom to shape the thermal profile during the real-time operation. Hence, in order to reduce the thermal stresses for paralleled GCIs, the power loss of each GCI is adjusted to shape the real-time thermal profile, where the $T_j$ swing and mean values are expected to be reduced. In the following section, the proposed thermal stress oriented dispatch (TSOD) strategy is described step by step to achieve the thermal stress reductions on all GCIs.

### A. THERMAL STRESS IDENTIFICATION

First, the instantaneous thermal stress of each GCI is identified. In some periods of the mission profile (MP), the generated power presents a mild variation, or even no variations. For those periods, GCI may remain in its original condition. However, for other periods, where the GCI suffers from a severe thermal stress, the proposed dispatch strategy is enabled to level the power loss and reduce the thermal stress. Hence, several criteria have been defined in following to identify the instantaneous thermal stress of each GCI first,

$$\overline{T_{j,i}}\,[k] > UB_i \tag{1}$$

$$\left|\Delta\overline{T_{j,i}}\,[k]\right| = \left|\overline{T_{j,i}}\,[k] - \overline{T_{j,i}}\,[k-1]\right| > D_i \tag{2}$$

where

$$UB_i = \Re \cdot UB_{i,\ \Re=1} \tag{3}$$

$$D_i = \Re \cdot D_{i,\ \Re=1} \tag{4}$$

$i$ denotes as the $i$th GCI, $\overline{T_j}$ is the mean value of the junction temperature over the fundamental period, which is estimated through the thermal model or indirectly measured through temperature-sensitive electrical parameters [35]. $UB$ and $D$ are defined as the upper bound and variation borders, respectively. In the proposed strategy, the lower bound border is not defined since it may increase the junction temperature mean value and adversely affect the thermal profile. The initial upper bound border $UB_{i,\Re=1}$ could be designed according to the maximum junction operating temperature of power modules or the specific application requirement. The initial variation border $D_{i,\Re=1}$ could be designed based on the junction temperature distribution over the power loading or the thermal cycling requirement, which is illustrated in Section III. $UB_i$ and $D_i$ also vary with the reliability $\Re$ of the $i$th GCI, where a more degraded GCI is expected to have lower $UB_i$ and $D_i$ in order to achieve a milder thermal profile. This correlation is one way proposed in this strategy. More well-designed correlations between the reliability and criterion parameters will be investigated in the future work.

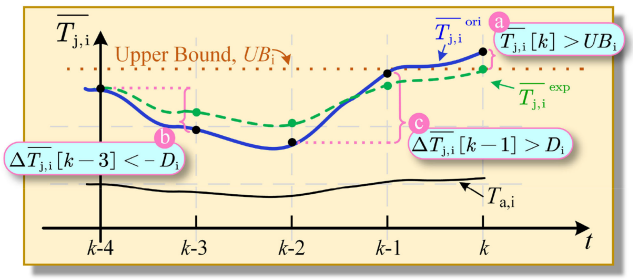


**FIGURE 2.** Design principles of the proposed centralized TSOD strategy.

Hence, the instantaneous thermal stress is regarded to be severe if (1) or (2) holds. Fig. 2 presents the design philosophy of the proposed TSOD strategy. $\overline{T_{j,i}}$, blue in Fig. 2, is used as the indicator to reflect the real-time thermal profile of the $i$th GCI. At each sampled instant $k$, the instantaneous thermal stress is identified. It turns out that at instants $k$, $k$-1 and $k$-3, the severe thermal stress occurs due to either (1) or (2) and corresponding situations are labeled by $a$, $b$ and $c$ in Fig. 2. In these cases, $i$th GCI will participate in the TSOD strategy for the thermal stress reduction.

### B. EXPECTED TEMPERATURE CALCULATION

For those GCIs participating in the dispatch strategy, their expected junction temperatures $\overline{T_{j,i}}^{exp}$ are then estimated. At any instant GCI exceeding either $UB$ or $D$ border, the proposed strategy would command the GCI to shape the real-time junction temperature close to the expected value in order to eliminate out-of-border periods. Then, the thermal stress will be ideally reduced and non-severe. Obviously, this expected value at least has to comply with criteria (1) and (2) to keep the GCI away from the severe thermal stress, which is adopted in the proposed strategy as follows,

$$\overline{T_{j,i}}^{exp}[k] = \begin{cases} UB_i, & \overline{T_{j,i}}\,[k] > UB_i \\ \overline{T_{j,i}}\,[k-1] - D_i, & \Delta\overline{T_{j,i}}\,[k] < -D_i \\ \overline{T_{j,i}}\,[k-1] + D_i, & \Delta\overline{T_{j,i}}\,[k] > +D_i \end{cases} \tag{5}$$

$\overline{T_{j,i}}^{exp}$ is the expected junction temperature by proposed TSOD strategy for $i$th GCI, which is shown in Fig. 2 in green. It is highly related to the $UB$ and $D$ borders from (5) because it depends on the way identifying the severity of the thermal stress. The expected junction temperature profile in Fig. 2 clearly presents a milder thermal profile than the one without the proposed TSOD strategy.

### C. EXPECTED LOSS CALCULATION

Once $\overline{T_{j,i}}^{exp}$ is derived, the expected power loss $P_{loss}{}^{exp}$ which is the required to generate $\overline{T_{j,i}}^{exp}$ needs to be determined. This can be estimated according to the $RC$ thermal network of the power module from the designed thermal management system. Usually, a simple heatsink temperature feedback, measured by a low-bandwidth thermocouple or a linear thermal sensor, is calibrated in industrial drives for the temperature monitoring and overtemperature protection. In the proposed

strategy, this real-time heatsink temperature is used to calculate the expected power loss below,

$$P_{\mathrm{loss,i}}^{\mathrm{exp}}[k] = \left(\overline{T_{\mathrm{j,i}}}^{\mathrm{exp}}[k] - T_{\mathrm{h,i}}[k]\right) / \left(\sum_{\mathrm{l}=1}^{\mathrm{n}} \frac{R_{\mathrm{th,l}}}{\tau_{\mathrm{l}} s + 1}\right) \tag{6}$$

where $R_{\mathrm{th,l}}$ and $\tau_{\mathrm{l}}$ are the thermal resistance and time constant for $l$th layer of the thermal network. The structure of the thermal network could be different depending on the specific thermal management system. In addition, in the daily or yearly reliability assessment, the thermal capacitance could be ignored since only the steady state of the temperature takes effect in these time scales, which is discussed in Section IV.

### D. DISPATCH ALGORITHMS

Then, the proposed TSOD strategy derives a new action to force the GCI to generate a power loss $P_{\mathrm{loss}}$ close to $P_{\mathrm{loss}}{}^{\mathrm{exp}}$ in order to achieve the expected junction temperature. This is where the local control level thermal stress reduction methods are imported. The power loss of power semiconductor devices, including the conduction loss $P_{\mathrm{loss}}{}^{\mathrm{cond}}$ and the switching loss $P_{\mathrm{loss}}{}^{\mathrm{swit}}$, is normally determined by (a) the mission profile, like the real power $P$ and reactive power $Q$, (b) the operating state of the converter, like the device voltage $V_{\mathrm{device}}$ and the conduction current $I_{\mathrm{c}}$, (c) the switching characteristics, like the switching frequency $f_{\mathrm{SW}}$ and the gate resistance $R_{\mathrm{G}}$, and (d) the junction temperature $T_{\mathrm{j}}$. However, not all of them can be adjusted from the control level. $R_{\mathrm{G}}$ is fixed in most of the industrial drives with no intelligent gate drive circuits. $T_{\mathrm{j}}$ is the goal in the proposed strategy and cannot be considered as the input action. $P$ is the generated power from the front-end mechanism and has to be transmitted stably all the time. $V_{\mathrm{device}}$ is related to the DC link voltage which is expected to be the nominal value as discussed in Section I. Hence, in the proposed TSOD strategy, $f_{\mathrm{SW}}$ and $Q$ are chosen to be two separate input actions to generate the expected power loss. The specific dispatch algorithms are described below.

#### 1) SWITCHING FREQUENCY VARIATION

Adjusting the switching frequency $f_{\mathrm{SW}}$ can feasibly control the switching loss during the normal operation and level the power loss over the mission profile. This switching frequency variation (SFV) method is employed as one approach to force the GCI to generate $P_{\mathrm{loss}}{}^{\mathrm{exp}}$.

In order to implement this method, the actual power loss has to be calculated first. Since the mean value of the junction temperature is used as the indicator to reflect the real-time thermal profile, the average power loss over the fundamental period is calculated. The conduction loss of the two-level three phases inverter as shown in Fig. 1 is calculated below,

$$P_{\mathrm{I}}^{\mathrm{cond}} = \left(\frac{1}{2\pi} + \frac{M\cos\theta}{8}\right) V_{\mathrm{I}} I_{\mathrm{pk}} + \left(\frac{1}{8} + \frac{M\cos\theta}{3\pi}\right) R_{\mathrm{I}} I_{\mathrm{pk}}^2 \tag{7}$$

$$P_{\mathrm{D}}^{\mathrm{cond}} = \left(\frac{1}{2\pi} - \frac{M\cos\theta}{8}\right) V_{\mathrm{D}} I_{\mathrm{pk}} + \left(\frac{1}{8} - \frac{M\cos\theta}{3\pi}\right) R_{\mathrm{D}} I_{\mathrm{pk}}^2 \tag{8}$$

where $P_{\mathrm{I}}{}^{\mathrm{cond}}$ and $P_{\mathrm{D}}{}^{\mathrm{cond}}$ represent the average conduction loss of the IGBT and the antiparallel diode, respectively, $M$ is the modulation index, $\theta$ is the phase shift of the grid voltage and the line current, $I_{\mathrm{pk}}$ is the magnitude of the current vector. $V_{\mathrm{I}}$, $R_{\mathrm{I}}$, $V_{\mathrm{D}}$, $R_{\mathrm{D}}$ are coefficients of the linear relationship of the I-V curve. After that, the switching loss is calculated through the behavioral loss model below,

$$P_{\mathrm{I}}^{\mathrm{swit}} = f_{\mathrm{SW}} \cdot \frac{1}{\pi}\left(E_{\mathrm{on}}\left(I_{\mathrm{pk}}\right) + E_{\mathrm{off}}\left(I_{\mathrm{pk}}\right)\right) \frac{V_{\mathrm{device}}}{V_{\mathrm{rated}}} \tag{9}$$

$$P_{\mathrm{D}}^{\mathrm{swit}} = f_{\mathrm{SW}} \cdot \frac{1}{\pi}\left(E_{\mathrm{rec}}\left(I_{\mathrm{pk}}\right)\right) \frac{V_{\mathrm{device}}}{V_{\mathrm{rated}}} \tag{10}$$

where $P_{\mathrm{I}}{}^{\mathrm{swit}}$ and $P_{\mathrm{D}}{}^{\mathrm{swit}}$ represent the average switching loss of the IGBT and the antiparallel diode, respectively, $E_{\mathrm{on}}$ and $E_{\mathrm{off}}$ are turn-on and -off switching energies of the IGBT at the rated voltage $V_{\mathrm{rated}}$. $E_{\mathrm{rec}}$ is the reverse recovery energy of the diode. More derivations of (7)-(10) can refer to [10]. Results of (7)-(10) are slightly modified according to the junction temperature due to the temperature dependent feature of the power loss.

It is observed that the switching frequency is linearly proportional to the average switching loss from (9) and (10) and as the input action in the proposed TSOD strategy, it is feasible to generate the expected power loss by only changing the switching frequency, which is a deterministic calculation below,

$$f_{\mathrm{SW,i}}[k] = \begin{cases} f_{\mathrm{SW,i}}[k-1] \cdot F_{\mathrm{i}}, & i \in B \\ f_{\mathrm{SW,i}}[k-1], & i \in G \end{cases} \tag{11}$$

$$f_{\mathrm{SW,i}}^{\mathrm{L}} \le f_{\mathrm{SW,i}} \le f_{\mathrm{SW,i}}^{\mathrm{H}} \tag{12}$$

where

$$F_{\mathrm{i}} = \frac{P_{\mathrm{I,i}}^{\mathrm{exp}}[k] + P_{\mathrm{D,i}}^{\mathrm{exp}}[k] - P_{\mathrm{I,i}}^{\mathrm{cond}}[k] - P_{\mathrm{D,i}}^{\mathrm{cond}}[k]}{P_{\mathrm{I,i}}^{\mathrm{swit}}[k] + P_{\mathrm{D,i}}^{\mathrm{swit}}[k]} \tag{13}$$

$P_{\mathrm{I}}{}^{\mathrm{exp}}$ and $P_{\mathrm{D}}{}^{\mathrm{exp}}$ are the expected power losses for the IGBT and the antiparallel diode, respectively. $F$ is the variation ratio of the switching frequency between the expected switching loss and the current switching loss, where the conduction loss remains the same. Then, the input action $f_{\mathrm{SW}}$ is updated by this ratio. $B$ is the set of GCIs participating in the TSOD strategy and $G$ is its complementary set. $f_{\mathrm{SW,i}}{}^{\mathrm{L}}$ and $f_{\mathrm{SW,i}}{}^{\mathrm{H}}$ are the lower and higher limits of the switching frequency for $i$th GCI, which are preset based on the system efficiency, the switching speed of the power semiconductor device, the harmonics, and the junction temperature. The result of (11) will be transmitted from the centralized TSOD strategy to the local controller in each dispatch iteration and the modulation scheme in the local controller will adjust the switching frequency as commanded.

### 2) REACTIVE POWER INJECTION

The reactive power $Q$ has validated its influence on the thermal profile in the literature [15], [16]. However, there is no specific strategy applying the reactive power injection (RPI) method to paralleled grid-connected inverters. This is attributed to the stability and scalability issues of this method. In the proposed centralized TSOD strategy, an optimization problem is formulated to make full use of RPI for paralleled GCIs and maintain the stable operation for the DER system.

Adjusting the reactive power would simultaneously change $M$, $\theta$, and $I_{\mathrm{pk}}$, which affects both the conduction and switching losses. From (7)-(10), it is noticed that it is not a simple linear relationship between the reactive power and the power loss. It would consume substantial online computation efforts to derive the deterministic results by knowing the expected power loss and solving the reactive power through (7)-(10) directly. In order to eliminate this issue and reduce the online calculation burden, a lookup table is established for each GCI to give a $Q$-$P_{\mathrm{loss}}$ mapping. Then, an optimization problem is defined below to calculate the input action $Q_{\mathrm{i}}$,

$$\min_{Q_{\mathrm{i}}} \quad \sum_{i\in B} \frac{\left(P_{\mathrm{loss,i}}\left(Q_{\mathrm{i}}\right) - P_{\mathrm{loss,i}}^{\mathrm{exp}}\left[k\right]\right)^2}{\left(P_{\mathrm{loss,i}}^{\mathrm{exp}}\left[k\right]\right)^2} \tag{14}$$

*s.t.*

$$\sum_{i\in B} Q_{\mathrm{i}} + \sum_{i\in G} Q_{\mathrm{i}} = Q_g \tag{15}$$

$$Q_{\mathrm{i}}^{-}\left[k\right] \le Q_{\mathrm{i}} \le Q_{\mathrm{i}}^{+}\left[k\right] \qquad \text{for } i \in B \tag{16}$$

where $P_{\mathrm{loss,i}}$ is derived through the lookup table for a certain $Q_{\mathrm{i}}$. $Q_{\mathrm{g}}$ is the total grid command on the reactive power which has to be maintained all the time. $Q_{\mathrm{i}}{}^{-}$ and $Q_{\mathrm{i}}{}^{+}$ confine the feasible range of the candidate reactive power. At different real power on the inverter, the available reactive power range is adapted according to either a current limit, or the grid code, or the thermal capacity of the inverter. Then, the optimal solution $Q_{\mathrm{i}}$ will be strictly within this range.

The objective function (14) can be solved by enumeration for a small number of GCIs or advanced quadratic programming algorithms, which provides a scalable implementation. The result of (14) will be transmitted from the centralized TSOD strategy to the local controller in each dispatch iteration and the local PI controller will control the $Q$ of the GCI as commanded.

### 3) FCS-MPC WITH REACTIVE POWER INJECTION

With significant features of the fast dynamic response, the nonlinear system formulation, and the multiple objectives and constraints integration, FCS-MPC has been widely investigated in power electronics systems [22]–[27]. Its capability for the thermal stress reduction is also explored in the local control level [19], [20]. With further investigation on FCS-MPC, it is found that not only $M$, $\theta$, and $I_{\mathrm{pk}}$ vary with the power flow, but also $f_{\mathrm{SW}}$ [21]. Hence, aiming at the FCS-MPC controlled GCIs, the proposed TSOD strategy uses the RPI method to alter $M$, $\theta$, $I_{\mathrm{pk}}$, and $f_{\mathrm{SW}}$ simultaneously and generate $P_{\mathrm{loss}}{}^{\mathrm{exp}}$.

Local FCS-MPC controller minimizes the current vector error in the problem formulation to realize the power flow control on GCIs. Only the current vector objective function from [20] is used for FCS-MPC in this paper. Similar to the reactive power injection for the PI controlled GCI, it is difficult to calculate the deterministic reactive power through the expected power loss for FCS-MPC. A new lookup table is built to give a $Q$-$P_{\mathrm{loss}}{}^{\mathrm{FCS\text{-}MPC}}$ mapping. The optimization problem formulation is updated as well,

$$\min_{Q_{\mathrm{i}}} \quad \sum_{i\in B} \frac{\left(P_{\mathrm{loss,i}}^{\mathrm{FCS-MPC}}\left(Q_{\mathrm{i}}\right) - P_{\mathrm{loss,i}}^{\mathrm{exp}}\left[k\right]\right)^2}{\left(P_{\mathrm{loss,i}}^{\mathrm{exp}}\left[k\right]\right)^2} \tag{17}$$

where $P_{\mathrm{loss,i}}{}^{\mathrm{FCS\text{-}MPC}}$ is derived through the new lookup table for a certain $Q_{\mathrm{i}}$. The objective function is then replaced by (17) and the rest of the problem formulation is the same. The result of (17) will be transmitted from the centralized TSOD strategy to the local controller in each dispatch iteration and the local FCS-MPC controller will control the $Q$ of GCI as commanded.

The procedure of the proposed centralized thermal stress oriented dispatch strategy ends up with sending the updated dispatch action to each local controller. Then, each local controller controls the GCI as commanded to generate the expected power loss to reduce the thermal stress. The complete block diagram of the proposed TSOD strategy is shown in Fig. 3. The flow chart of the centralized TSOD strategy is presented for both PI and FCS-MPC controlled GCIs. The loss and thermal models of power modules are used to estimate the real-time junction temperature locally. The converter information, including the mean value of the junction temperature $\overline{T_{\mathrm{j,i}}}$, the heatsink temperature $T_{\mathrm{h}}$, the real and reactive power $P$ and $Q$, are collected and transmitted to the centralized TSOD strategy.

A holistic time scale is also presented in Fig. 3 ranging from microseconds to megaseconds. It shows a comprehensive time scaling frame in the centralized-TSOD-strategy-integrated DER systems. The dispatch period $T_{\mathrm{dis}}$ of the proposed TSOD strategy is suggested to be smaller than the time constant of the temperature transient response of power modules, which would interfere with the rise or fall of the junction temperature timely, and larger than the fundamental period of the electrical system in order to cover the variation of the instantaneous estimated junction temperature. Besides, the smaller $T_{\mathrm{dis}}$ requires more data rate from the communication network, which is a tradeoff and might be a potential limit. The proposed centralized TSOD strategy is implemented on a four-paralleled-GCIs platform and its performance is evaluated in Section III and IV.

In the rest of the paper, results from different methods are named in the following for the convenience in the analysis,

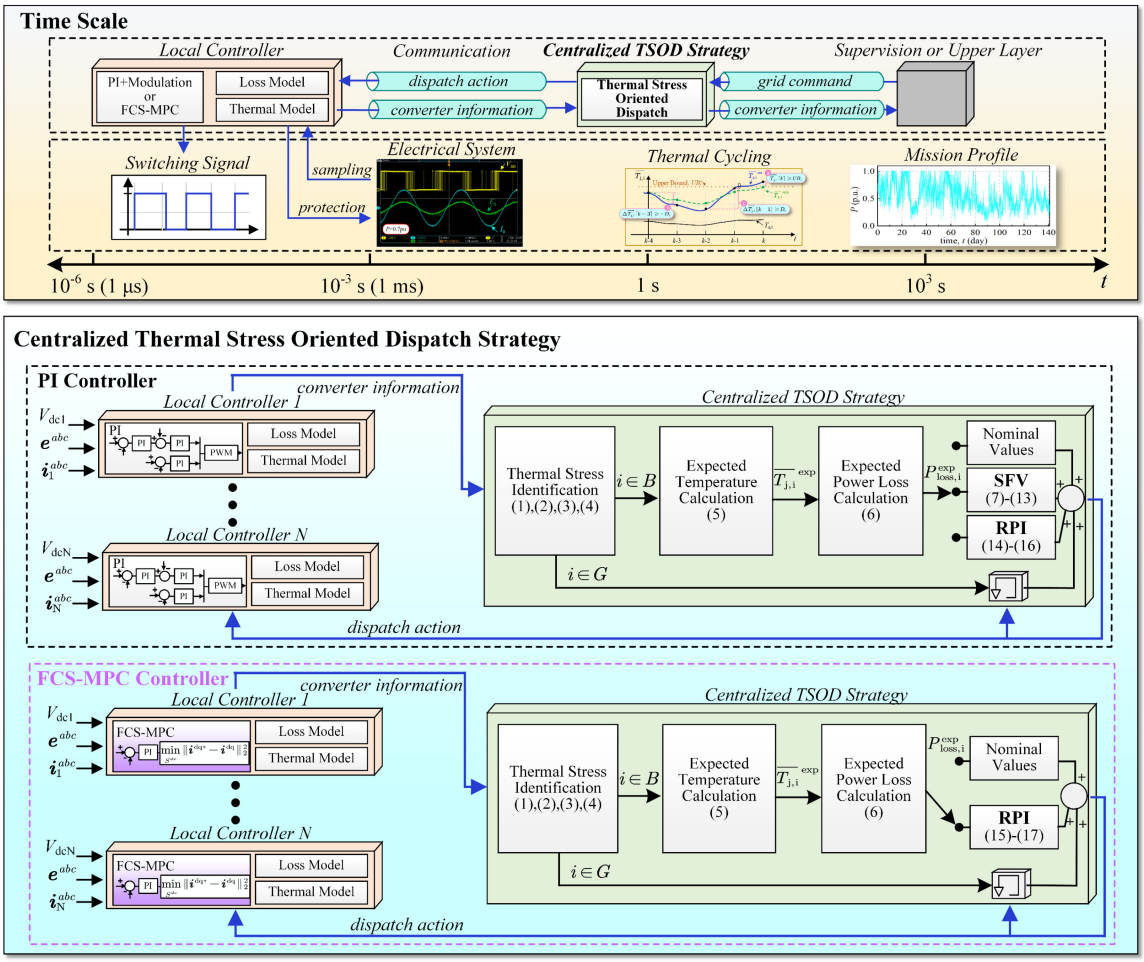


**FIGURE 3.** System diagram and time frame of the proposed centralized TSOD with different dispatch algorithms for PI and FCS-MPC local controllers.

| | |
|---|---|
| *PI* | PI-controlled GCI with nominal values and no TSOD strategy |
| *TSOD-SFV-PI* | PI-controlled GCI with TSOD strategy and $f_{sw}$ dispatch action |
| *TSOD-RPI-PI* | PI-controlled GCI with TSOD strategy and $Q$ dispatch action |
| *FCSMPC* | FCS-MPC-controlled GCI with nominal values and no TSOD strategy |
| *TSOD-RPI-FCSMPC* | FCS-MPC-controlled GCI with TSOD strategy and $Q$ dispatch action |

## III. REAL-TIME SIMULATION VERIFICATION

To verify the effectiveness of the proposed centralized TSOD strategy, a four-paralleled-GCIs platform is established in the real-time Model-in-the-Loop (MIL) testing. This four-paralleled-GCIs platform is introduced from the reference model of the ocean current energy converter (OCEC) system [28], as shown in Fig. 4(a). The OCEC system can be planned as the DER system like the wind power. The power electronics systems housing nacelle in Fig. 4(a) contains four ABB ACS800-17-0790-7 industrial drives in parallel. Each of them is connecting to one electric machine and transmits the power to the point-of-common-coupling (PCC). The circuit diagram on the grid side of the industrial drive is highlighted and displayed in Fig. 4(b). Six ABB HiPak 5SND 0800M170100 IGBT modules (1700V/800A/125 °C) [33] are used for each two-level three-phase GCI. Identical line reactors are connected to all GCIs. The system parameters are listed all in Table I.

**TABLE I** Parameters of One Power Chain of the OCEC System

| | |
|---|---|
| Rated power $P$ | 900 kW/ 1 p.u. |
| Rated reactive power $Q_g$ | 0 kvar |
| Rated DC bus voltage $V_{dc}$ | 1100 V |
| Grid frequency $f$ | 60 Hz |
| Rated AC grid voltage $\boldsymbol{e}^{abc}$ | 690 V |
| Line current $\boldsymbol{i}^{abc}$ | 753 A |
| Line inductance $L_g$ | 0.4 mH |
| Line resistance $R_g$ | 10 mΩ |
| Junction temperature $T_j$ | -40~125ºC, 150ºCmax |
| Air flow | 6400 $m^3$/h |
| Air temperature $T_{air}$ | 25 ºC |
| IGBT case-heatsink $R_{th}$ | 24 K/kW |
| Diode case-heatsink $R_{th}$ | 48 K/kW |
| Heatsink-ambient $R_{th}$ | 20 K/kW |

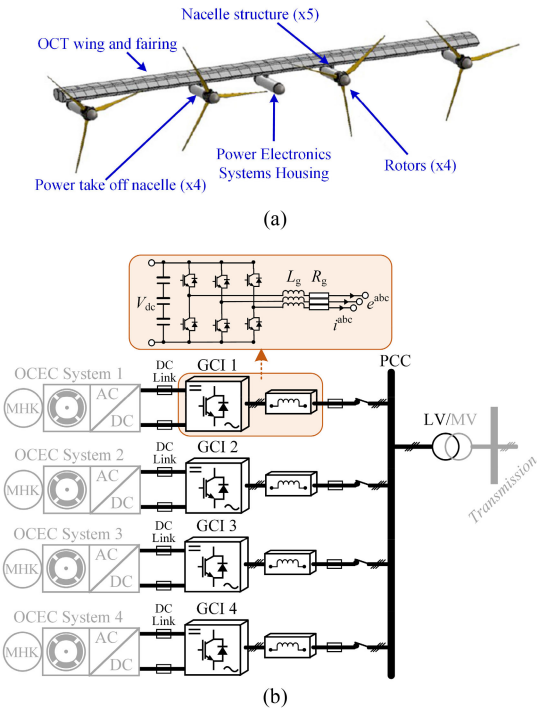


**FIGURE 4.** Four-paralleled GCIs platform, (a) the reference model from [28] and (b) the circuit diagram.

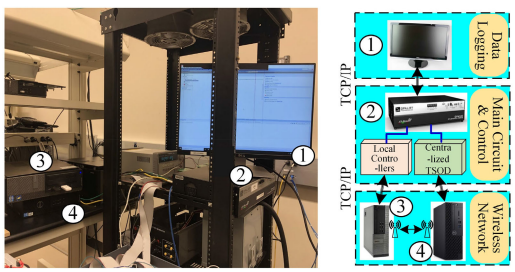


**FIGURE 5.** Real-time MIL test platform based on RT-Lab.

Fig. 5 shows the MIL test platform, which is based on the Opal-RT real-time simulator. PI linear controllers and FCS-MPC controllers are calibrated separately for four GCIs and the same sampling period 50 $\mu$s is adopted for both. The nominal switching frequency in the PI controller is 2.5 kHz which is the mean value of the variable switching frequency results by FCS-MPC controller over the power loading. The switching frequency dispatch command for TSOD-SFV-PI ranges from 1 kHz to 5 kHz, which equals to the autonomous switching frequency variation by FCS-MPC. The reactive power dispatch command for TSOD-RPI-PI and TSOD-RPI-FCSMPC in this paper is limited by the system power rating at different real power. Other control parameters are listed in Table II. The proposed centralized thermal stress oriented dispatch strategy is built with a one-second dispatch period, the 125 °C-upper-bound border and the 10 °C-variation border, where the 125 °C-upper-bound border comes from the maximum operating junction temperature provided from the

**TABLE II** Parameters of the Local PI and FCS-MPC Controllers

| | |
|---|---|
| PI Linear Controller | |
| Sampling period $T_s$ | 50 µs |
| Nominal command $Q_i$ | 0 kvar |
| Nominal $f_{SW}$ | 2500 Hz |
| Switching frequency range | [1000 Hz, 5000 Hz] |
| FCS-MPC Controller | |
| Sampling period $T_s$ | 50 µs |
| Prediction receding horizon $H$ | 1 |
| Nominal command $Q_i$ | 0 kvar |

**TABLE III** Parameters of the Proposed Centralized TSOD Strategy

| | |
|---|---|
| Dispatch period $T_{dis}$ | 1 s |
| Initial reliability $\Re_i$ | 1 |
| Upper bound border $UB_i$ | 125°C |
| Variation border $D_i$ | 10°C |

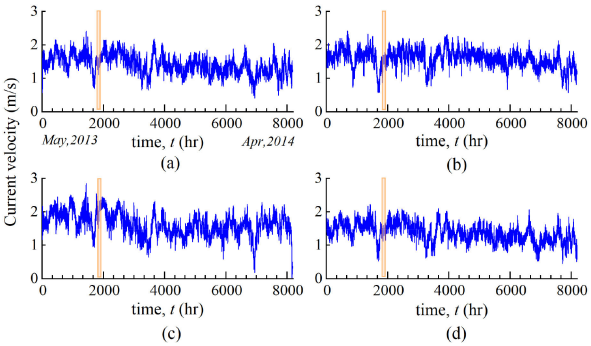


**FIGURE 6.** Yearly mission profiles of ADCPs in Gulf Stream, Florida, USA.

**TABLE IV** Dispatch Commands from the Proposed Centralized TSOD Strategy

| | TSOD-SFV-PI, $f_{SW}$ (kHz) | | TSOD-RPI-PI, $Q$ (kvar) | |
|---|---|---|---|---|
| | 1st | 2nd | 1st | 2nd |
| $t$ (s) | 601 | 1201 | 601 | 1201 |
| GCI1 | 3.3 | 2.6 | 240 | -180 |
| GCI2 | 3.4 | 2.2 | 280 | 80 |
| GCI3 | 3.5 | 2.1 | -520 | 100 |
| GCI4 | 2.6 | 2.1 | 0 | 0 |

datasheet [33] and the 10 °C-variation border comes from the junction temperature difference between 0.1 p.u. power loading change. Other TSOD strategy parameters are listed in Table III. Four yearly mission profiles of the current velocity are imported from moored acoustic doppler current profiles (ADCPs) which are deployed in Gulf Stream, Florida, USA from May 2013 to April 2014 in Fig. 6 [34]. One-hour data with the 15-minutes interval of these MPs are used to demonstrate the proposed TSOD strategy in the MIL testing. These MPs are translated to power loadings through the rotor power coefficient in [28].

Fig. 7 shows results of the real power and the junction temperatures for four GCIs, where PI linear controllers are used to regulate these GCIs. All dispatch actions calculated from the centralized TSOD strategy are listed in Table IV. Dispatch commands are updated twice for both SFV and RPI. When

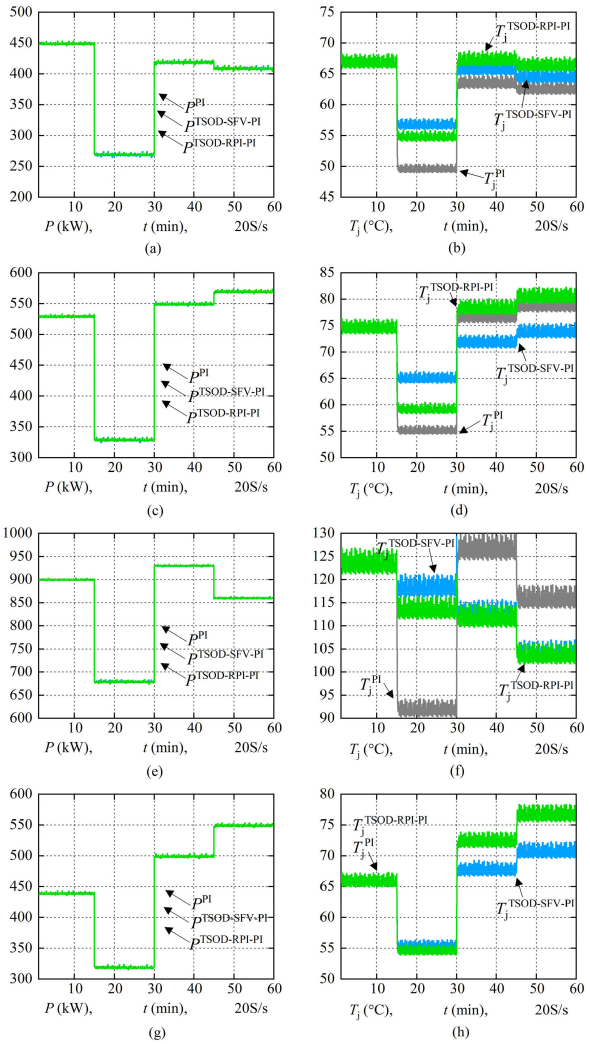


**FIGURE 7.** MIL results of the power flow (left) and the IGBT junction temperature (right) for PI-controlled (a) and (b) GCI 1, (c) and (d) GCI 2, (e) and (f) GCI 3, (g) and (h) GCI 4.

$f_{SW}$ is used as the dispatch command, the reactive power of all GCIs is fixed at the nominal value and vice versa.

Fig. 7(a), (c), (e), and (g) present the power flow control without and with the TSOD strategy. From the overlapped waveforms, it is noted that the proposed TSOD strategy with either SFV or RPI does not affect the normal real power transmission. DER systems are maintained in the stable condition all the time. Fig. 7(b), (d), (f), and (h) present the junction temperatures of the IGBTs. From the 15th min, the conventional junction temperature experiences a huge fall for all GCIs due to the power dip from MPs. However, with the assistance of the TSOD strategy, the junction temperature is prevented from such a huge temperature drop. For TSOD-SFV-PI, the junction temperatures (blue in Fig. 7) are roughly limited by 10 °C-steady-state variation and under 125 °C border all the time because of the updated switching loss. For TSOD-RPI-PI, the junction temperatures (green in Fig. 7) for most GCIs display a smaller drop than the one without the TSOD

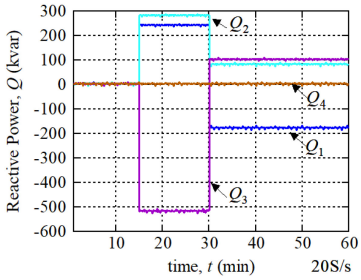


**FIGURE 8.** Reactive power dispatch commands for PI-controlled GCIs.

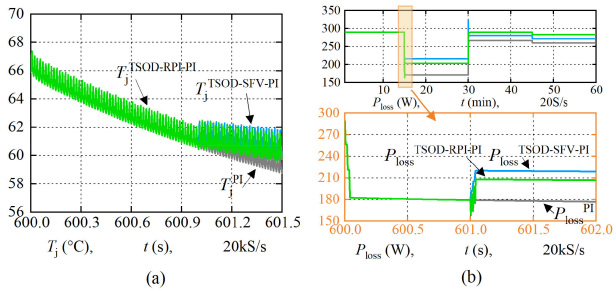


**FIGURE 9.** Transient response of the proposed centralized TSOD strategy.

strategy. However, the temperature profile is not strictly within the 10 °C-steady-state variation border as SFV does. This is because, according to the dispatch algorithm in Section II, RPI outputs the optimal reactive power by minimizing (14), which may not provide the absolute expected power loss from (6) and present a compromised performance for most GCIs. The total reactive power is maintained at the grid command $Q_g$ in Fig. 8.

Fig. 9 displays the response of the proposed TSOD strategy for GCI1 on the IGBT junction temperature and power loss from 600s to 601.5s, where the real power drops from 450 kW to 270 kW at 600s. At 601s, the TSOD strategy detects the severe thermal stress on GCI1, and then, the updated command (SFV: 3.3-kHz $f_{SW}$ or RPI: 240-kvar $Q$) is transmitted to GCI1. With the updated command, the new power loss of one IGBT increases from 170 W to 215 W by SFV and to 203 W by RPI and then, the TSOD strategy successfully interferes with the junction temperature of GCI1 by preventing from a huge drop.

Fig. 10 shows results of the real power and the junction temperatures for four GCIs, where FCS-MPC controllers are used to regulate GCIs. All dispatch actions calculated from the centralized TSOD strategy are listed in Table V. Dispatch commands are updated twice for only RPI in this case.

Fig. 10(a), (c), (e), and (g) present the power flow control without and with the TSOD strategy. From overlapped waveforms, the real power transmissions in DER systems are also guaranteed all the time for FCS-MPC controlled converters with the proposed TSOD strategy. Fig. 10(b), (d), (f), and (h) present the junction temperatures of the IGBTs. It is observed that with no assistance of the TSOD strategy, the junction temperature results by FCS-MPC controlled GCIs present a

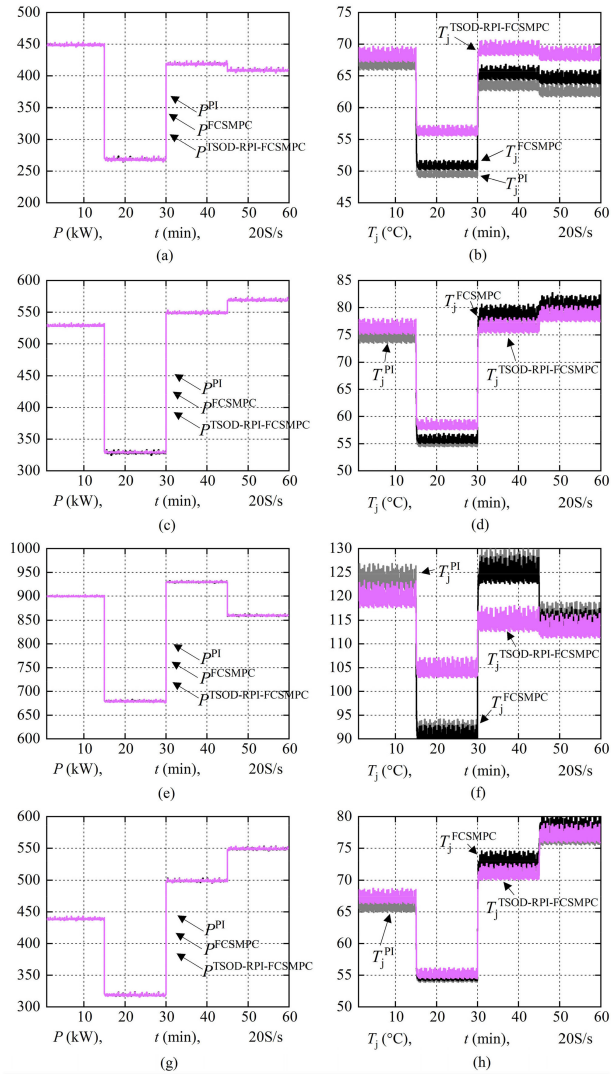


**FIGURE 10.** **MIL results of the power flow (left) and the IGBT junction temperature (right) for FCSMPC-controlled (a) and (b) GCI 1, (c) and (d) GCI 2, (e) and (f) GCI 3, (g) and (h) GCI 4.**

**TABLE V** **Dispatch Commands from the Proposed Centralized TSOD Strategy**

| | TSOD-RPI-FCSMPC, $Q$ (kvar) | |
|---|---|---|
| | 1st | 2nd |
| $t$ (s) | 601 | 1201 |
| GCI1 | -150 | -120 |
| GCI2 | 320 | 20 |
| GCI3 | -220 | 30 |
| GCI4 | 50 | 70 |

slight difference from the ones by PI, which is attributed to the variable switching frequency property of FCS-MPC. Then, with the assistance of the TSOD strategy (purple in Fig. 10), the junction temperature is further prevented from a huge temperature drop at 15 mins. However, similar to the TSOD-RPI for PI controlled GCIs, the temperature profile is not strictly within the 10 °C-steady-state variation border. Besides, the dispatch commands in Table V are different from

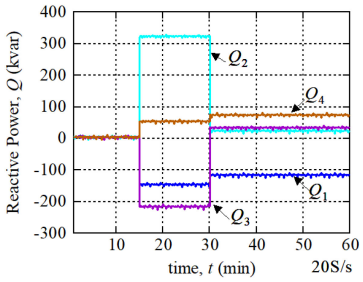


**FIGURE 11.** **Reactive power dispatch commands for FCS-MPC-controlled GCIs.**

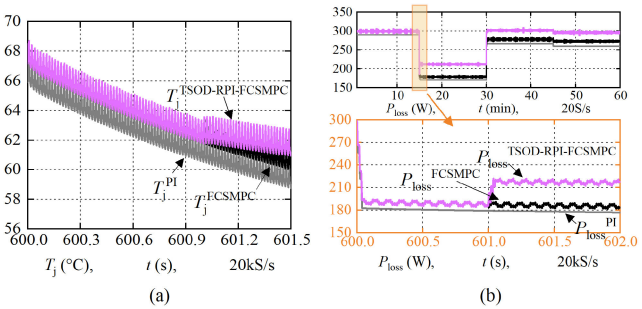


**FIGURE 12.** **Transient response of the proposed centralized TSOD strategy.**

the ones in Table IV, since in FCS-MPC, the $f_{SW}$ also varies with the operating point of the converter. Hence, the reactive power injection offers more freedoms on the power loss adjustment, whereas the total reactive power is maintained at $Q_g$ as well in Fig. 11.

Fig. 12 displays the response of the proposed TSOD strategy for FCS-MPC controlled GCI1 from 600s to 601.5s. At 601s, the TSOD strategy detects the severe thermal stress of GCI1 again, where both temperature values at 601s and 600s are higher than the ones by PI controlled GCI1, but still beyond the variation border. Then, the updated command (RPI: −150-kvar $Q$) is transmitted to GCI1. With the updated command, the new power loss of one IGBT increases from 190 W to 218 W and then, the TSOD strategy successfully interferes with the junction temperature of GCI1 by preventing from a huge drop.

From all MIL results, it is clearly illustrated that the junction temperature is prevented from decreasing to a very low value by proposed centralized TSOD strategy for both PI and FCS-MPC controlled GCIs. A more balanced power loss is achieved for all paralleled inverters by updating the dispatch commands, either $f_{SW}$ or $Q$.

## IV. RELIABILITY ASSESSMENT AND TRADEOFF ANALYSIS

In order to further verify the effectiveness of the thermal stress reduction, investigate the impact of the proposed TSOD strategy on the lifetime and reliability of IGBTs, and compare different performances between PI and FCS-MPC local controllers, the reliability assessment and the tradeoff analysis are conducted in this section.

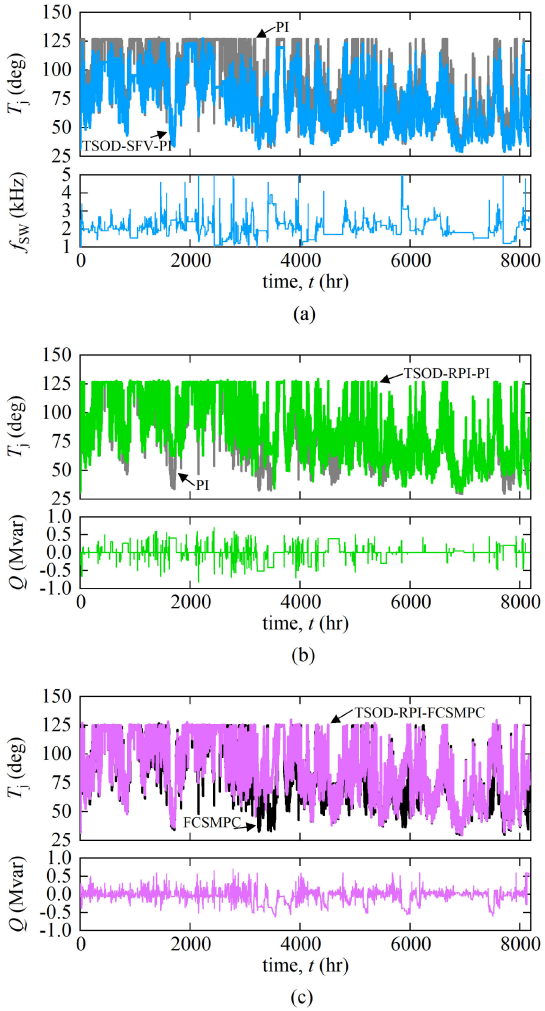


**FIGURE 13. Yearly thermal profiles by reliability assessment for (a) PI and TSOD-SFV-PI, (b) PI and TSOD-RPI-PI, and (c) FCSMPC and TSOD-RPI-FCSMPC.**

The yearly mission profiles from Fig. 6 are adopted for the same four-paralleled-GCIs platform. Because the reliability assessment is a long-term profile investigation, the short-term responses including the transient states on the DC link voltage and the line currents, the thermal capacitance, and the small time step are reasonably ignored [2]. The identical parameters of the DER systems, the local controllers, and the proposed centralized TSOD strategy from Table I, II, and III are used in the reliability assessment. Results are presented below in terms of the thermal profile, the thermal cycles, and the accumulative damage and predicted lifetime of IGBTs.

### A. YEARLY THERMAL PROFILES

Applying the proposed thermal stress oriented dispatch strategy to the yearly mission profiles derives the yearly thermal profiles. Fig. 13 presents yearly junction temperature profiles of IGBT in GCI1, where the results of PI controlled GCI1 are displayed in Fig. 13(a) and (b) and results of FCS-MPC controlled GCI1 are displayed in Fig. 13(c). It is observed that with the proposed TSOD strategy, the thermal profiles are all shaped in order to reduce the thermal stress.

Fig. 13(a) presents the yearly thermal profile by PI and TSOD-SFV-PI. Compared with the conventional profile, the shaped thermal profile achieves a lower junction temperature for most high power loading instants. In some of low power loading instants, the junction temperature also increases in order to reduce the swing value in the thermal cycling. This is attributed to the switching frequency variation in the PI controller, that the switching loss can be adjusted higher or lower in any direction.

Fig. 13(b) presents the yearly thermal profile by PI and TSOD-RPI-PI. Compared with the conventional profile, the shaped thermal profile achieves a higher junction temperature for most low power loading instants and the same temperature level for the high power loading instants. This is attributed to the lowest power loss at zero reactive power in the PI controller, that the power loss can only be adjusted to a higher level. Hence, the junction temperature swing value has been reduced by increasing the low level of the thermal profile, and the mean value has been sacrificed in return. Similar case happens to Fig. 13(c) by TSOD-RPI-FCSMPC. However, since the $f_{SW}$ varies with the reactive power, FCS-MPC provides more flexibilities on the power loss adjustment, where the lowest power loss may not be at zero reactive power operating point. Thus, the thermal profile by TSOD-RPI-FCSMPC is different from the one by TSOD-RPI-PI from Fig. 13.

### B. THERMAL CYCLES COUNTING

Once receiving all thermal profiles for four GCIs, the rainflow counting algorithm, which is a widely used counting method in the fatigue study, is employed to discretize the thermal profile in terms of the junction temperature mean value $\overline{T_j}$, the swing value $\Delta T_j$, and the cycling period $t_{cycle}$, which later are fit into the IGBT lifetime prediction model.

Fig. 14 displays the rainflow counting results from thermal profiles in Fig. 13 for GCI1. The colormap reflects the number of the thermal cycles based on two variables, the temperature mean value (Y axis) and swing value (X axis). The red arrow reflects the shift direction of thermal cycles compared to the one by PI controlled GCI without the proposed TSOD strategy. Fig. 14(b) shows the colormap for TSOD-SFV-PI, where more cycles exist in the lower-mean-value and lower-swing-value squares. The number of cycles beyond criteria (1) and (2) is significantly reduced. Fig. 14(c) shows the colormap for TSOD-RPI-PI, where more cycles exist in the higher-mean-value and lower-swing-value squares. This is compliant with the thermal profile in Fig. 13(b), that the temperature swing value has been reduced by increasing the low level of the thermal profile, and the mean value has been sacrificed in return. Fig. 14(d) and (e) display the colormaps for the FCS-MPC and TSOD-RPI-FCSMPC. Without the assistance of TSOD strategy, Fig. 14(d) illustrates more moderate thermal cycles than Fig. 14(a), where more cycles are located in the lower-mean-value squares. With TSOD strategy in Fig. 14(e), more cycles move to the lower-swing-value squares.

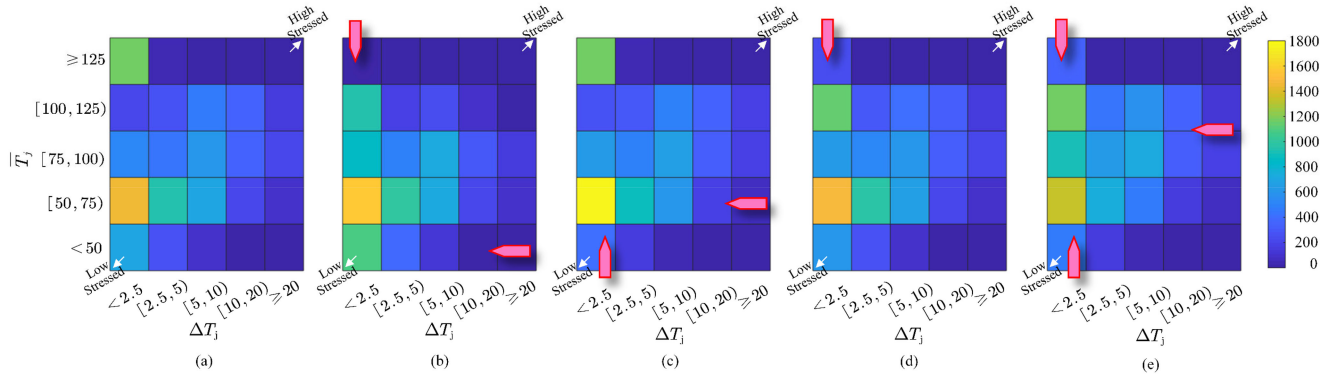


**FIGURE 14.** Thermal cycles counting results for (a) PI, (b) TSOD-SFV-PI, (c) TSOD-RPI-PI, (d) FCSMPC, and (e) TSOD-RPI-FCSMPC.

From the comparison between these colormaps, more thermal cycles are located in the lower-mean-value and lower-swing-value squares by proposed TSOD strategy, which contributes to a reduced thermal stress on IGBTs. The FCS-MPC controlled GCI performs a more mitigated thermal stress than the one by PI, even if no TSOD strategy is engaged.

### C. ACCUMULATIVE DAMAGE AND LIFETIME PREDICTION

A more straightforward comparison comes from the accumulative damage and predicted lifetime on the IGBTs. Particularly for those TSOD-RPI results, where more thermal cycles exist in the higher-mean-value and lower-swing-value squares, the quantified results can give an intuitive judgment on whether the thermal stress is indeed reduced by proposed TSOD strategy. Hence, the Bayerer's IGBT lifetime model [29] and Miner's rule [30] are used to calculate the accumulative damage (AD) and the predicted lifetime based on the thermal cycles counting results,

$$N_{\mathrm{f}} = A\left(\Delta T_{\mathrm{j}}^{-\beta_1}\right) \cdot \exp\left(\frac{\beta_2}{\overline{T}_{\mathrm{j}} + 273}\right) t_{\mathrm{cycle}}^{\beta_3} I^{\beta_4} V^{\beta_5} D^{\beta_6} \quad (18)$$

$$\mathrm{AD} = \sum_i \frac{n_i}{N_{\mathrm{f},i}} \quad (19)$$

where $N_{\mathrm{f}}$ is defined as the number of cycles to failure for the specific thermal stress ($\overline{T}_{\mathrm{j}}$, $\Delta T_{\mathrm{j}}$, $t_{\mathrm{cycle}}$), $n_{\mathrm{i}}$ is the number of this thermal stress, $I$ is the current per wire bond, $V$ is the voltage class, and $D$ is the diameter of the bond wire. Parameters $A$ and $\beta_{1\text{-}6}$ are device dependent constants according to the aging data provided by manufacturers [31]. The lifetime prediction is calculated by reciprocal of AD. When AD goes to one, the device is regarded to be fully failure out.

Fig. 15 presents ADs by mission profiles in Fig. 6 and predicted lifetimes of the IGBT for all four GCIs. The lifetime of the IGBT by PI-controlled GCIs without the proposed TSOD strategy is set to be around 10 years as the benchmark. It is clearly shown that the IGBTs in almost all GCIs achieve a less accumulative damage and a more predicted lifetime with the proposed TSOD strategy. Among all, TSOD-SFV-PI gives the least ADs and the longest lifetime of 13∼15 years for all

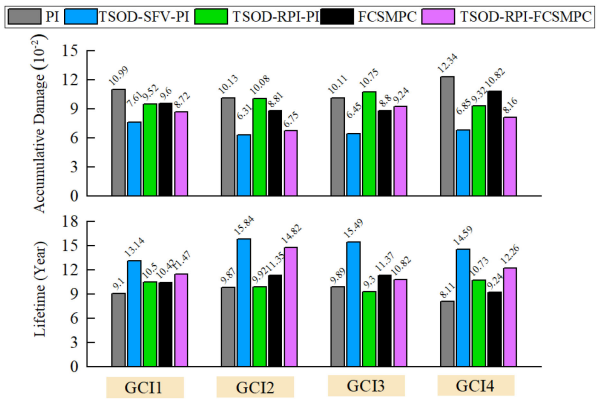


**FIGURE 15.** Accumulative damages and predicted lifetimes for all GCIs.

**TABLE VI** Annual Energy Productions and Total Platform Efficiency

| | Annual Energy Productions (MWh) | | | | η(%) |
|---|---|---|---|---|---|
| Method | GCI1 | GCI2 | GCI3 | GCI4 | Total |
| PI | 4683 | 6043 | 5919 | 4398 | 97.65 |
| TSOD-SFV-PI | 4702 | 6073 | 5950 | 4416 | 98.10 |
| TSOD-RPI-PI | 4677 | 6043 | 5918 | 4393 | 97.59 |
| FCSMPC | 4683 | 6046 | 5921 | 4398 | 97.67 |
| TSOD-RPI-FCSMPC | 4676 | 6044 | 5919 | 4388 | 97.58 |

GCIs. Without the TSOD strategy, FCS-MPC controlled GCIs perform a slightly longer lifetime of 10∼11 years than the ones by PI controlled GCIs. TSOD-RPI-FCSMPC performs even better. It is admitted that the accuracy of the IGBT lifetime model has been an open topic, which can be validated through power cycling acceleration tests in the laboratory. However, in this study, the relative changes on the AD and the lifetime are more of the interest and clear to verify the effectiveness of the proposed TSOD strategy and compare different methods.

### D. TRADEOFF ANALYSIS

Since the essential idea of the proposed TSOD strategy is to balance the power loss for the thermal stress reduction, the annual energy production and the system efficiency are affected if the TSOD strategy engages. Table VI lists the annual energy productions for all four GCIs and the total platform

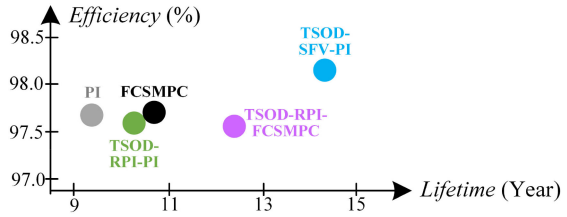


**FIGURE 16.** Lifetime and efficiency comparison between different methods.

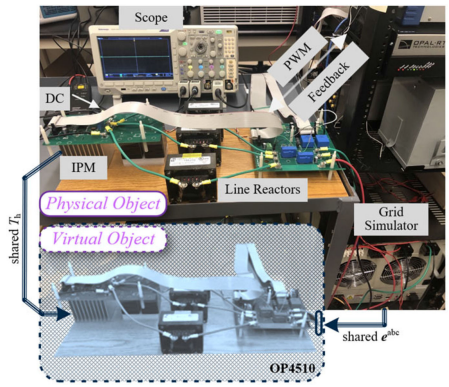


**FIGURE 17.** Digital twin hardware platform for the experimental testing.

energy efficiency. The benchmark of the power efficiency is set to be 98%-max value at 770 kW with nominal $Q$ and $f_{SW}$ values [32]. It is noted that the TSOD-SFV-PI method contributes to the largest annual energy productions (total in 21,141 MWh) and the highest efficiency (98.10%), which are attributed to the lower power loss by decreasing the switching frequency. Without the proposed TSOD strategy, FCS-MPC controlled GCIs perform higher annual energy productions and the efficiency (total in 21,048 MWh, 97.67%) than ones by PI controlled GCIs (total in 21,043 MWh, 97.65%), which are attributed to the switching frequency variation property of FCS-MPC, where a lower switching frequency is derived at the higher power loading autonomously. Both TSOD-RPI-PI and -FCSMPC methods downgrade the annual energy productions and the total platform efficiency, since in most of interfered instants, it generates more power losses to reduce the temperature swing value.

Fig. 16 presents the averaged lifetime and energy efficiency tradeoff between different methods. It is observed that for PI controlled GCIs, TSOD-SFV-PI method gives the best performances on both the lifetime and efficiency, which offers the DER system a strong motivation to implement the proposed strategy. For FCS-MPC controlled GCIs, TSOD-RPI-FCSMPC also shows a better performance on the lifetime, where the sacrificed efficiency can certainly be compensated by a saved cost on the longer operating lifetime.

## V. EXPERIMENTAL VERIFICATION

A digital twin hardware platform is developed in Fig. 17 to validate the effectiveness of the proposed centralized TSOD strategy as well. It contains a physical object (PO) of a downscale grid-connected inverter and a virtual object (VO) of the identical inverter in parallel. PO and VO share the grid voltage $\boldsymbol{e}^{abc}$ and the measured heatsink temperature $T_h$ in the real-time operation. Local PI and FCS-MPC controllers are calibrated separately. The nominal switching frequency in the PI controller is 8 kHz which is designed to be the mean value of the variable switching frequency results of FCS-MPC over the power loading [21]. All experimental parameters are presented in Table VII and VIII, including the inverter, the local controllers and the designed TSOD strategy. The upper bound and variation borders are set to be 100 °C and 10 °C, respectively, at every one-second dispatch period. The similar varying mission profiles from Fig. 18 are loaded on PO and VO simultaneously. The proposed centralized TSOD strategy is applied at 26 min.

Fig. 19 displays the dispatch action results of TSOD-SFV-PI, TSOD-RPI-PI, and TSOD-RPI-FCSMPC, respectively. It is noted that all dispatch algorithms take effect in experiments. For SFV in Fig. 19(a), the switching frequency value varies within the range between 5 kHz and 10 kHz. For RPI in Fig. 19(b) and (c), the proposed TSOD strategy stably maintains the total reactive power at zero all the time and limits their power flow within the rated design 1.4 kVA. Fig. 20 and 21 show the estimated IGBT loss under dispatch actions

**TABLE VII** Parameters of the GCI in the Experiments for Both PO and VO

| | |
|---|---|
| Rated power $S$ | 1.4 kVA/ 1 p.u. |
| Rated DC bus voltage $V_{dc}$ | 200 V |
| Grid frequency $f$ | 60 Hz |
| Rated AC grid voltage $\boldsymbol{e}^{abc}$ | 46.2/80 V |
| Line Reactors $L_g$ $R_g$ | 8 mH, 0.3 Ω |
| IGBT module | Infineon IKCM15L60GD [36] |
| Sampling period $T_s$ | 25 μs |

**TABLE VIII** Parameters of the Local Controllers and TSOD Strategy

| | |
|---|---|
| PI Linear Controller | |
| Nominal command $Q_i$ | 0 var |
| Nominal $f_{SW}$ | 8000 Hz |
| Switching frequency range | [5000 Hz, 10000 Hz] |
| FCS-MPC Controller | |
| Prediction receding horizon $H$ | 1 |
| Nominal command $Q_i$ | 0 var |
| Centralized TSOD Strategy | |
| Dispatch period $T_{dis}$ | 1 s |
| Initial reliability $\Re_i$ | 1 |
| Upper bound border $UB_i$ | 100°C |
| Variation border $D_i$ | 10°C |

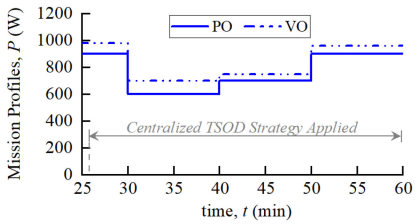


**FIGURE 18.** The 30-minutes mission profiles for the hardware platform.

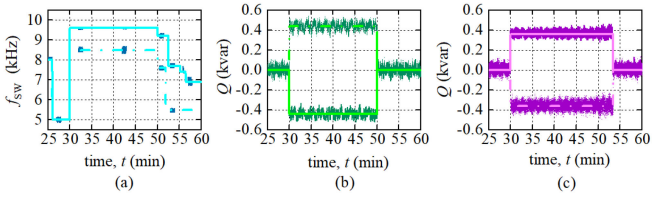


**FIGURE 19.** Dispatch actions of the centralized TSOD strategy for PO (solid line) and VO (dash line), (a), TSOD-SFV-PI, (b), TSOD-RPI-PI, (c) TSOD-RPI-FCSMPC.

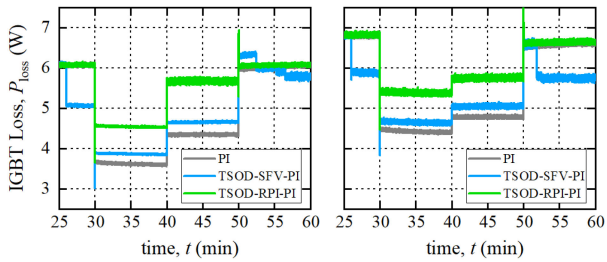


**FIGURE 20.** IGBT loss for PO (left) and VO (right) with local PI controller.

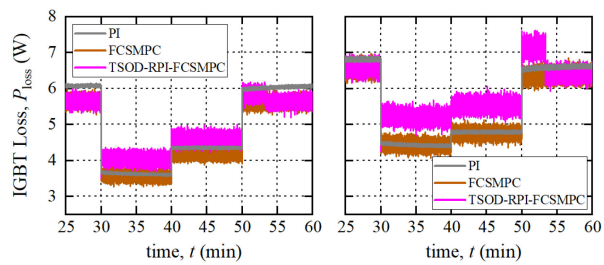


**FIGURE 21.** IGBT loss for PO (left) and VO (right) with FCS-MPC controller.

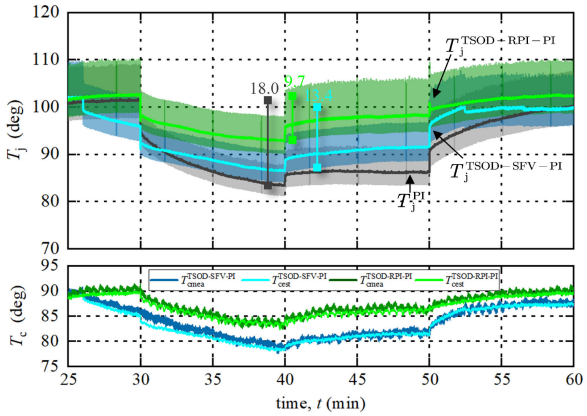


**FIGURE 22.** Estimated junction, estimated and measured case temperatures of PO with local PI controller for PI (gray), TSOD-SFV-PI (blue), and TSOD-RPI-PI (green).

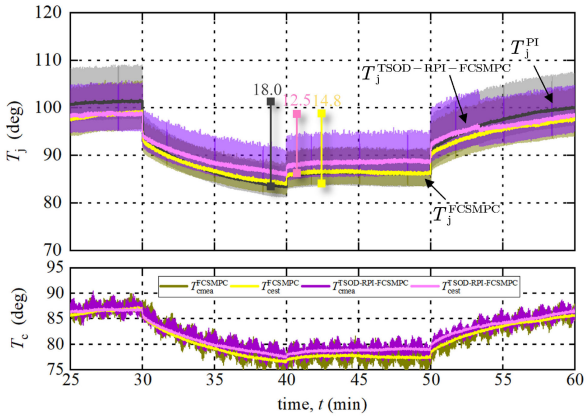


**FIGURE 23.** Estimated junction, estimated and measured case temperatures of PO with local FCS-MPC controller for FCSMPC (yellow) and TSOD-RPI-FCSMPC (purple).

for PI controlled and FCS-MPC controlled GCIs, respectively. All IGBT losses with the proposed TSOD strategy are more balanced than the one without the TSOD strategy, even though at few time intervals the IGBT loss may be found higher than the highest value or lower than the lowest value of the conventional PI or FCS-MPC result. This is highly acceptable because the temperature transient response is much slower than the electrical one. The power loss has been balanced in advance of the severe temperature variation. In other words, the proposed centralized TSOD strategy timely interferes with the rise or fall of the temperature and effectively reshape the thermal profile.

Eventually, Fig. 22 and 23 present the thermal profile results of PO, where the estimated junction temperature of the IGBT $T_j$, the estimated and the measured case temperatures of the power module, $T_{cest}$ and $T_{cmea}$, are shown. The estimated values come from the thermal model in the local controller and a measured heatsink temperature feedback. The background envelops in both Fig. 22 and 23 are instantaneous estimated junction temperatures. Since the transient response of the temperature is much smaller than the electrical one, its average value is more of the interest, which is highlighted in front. It is observed that with the TSOD strategy, the junction temperatures have less variations compared to the one without the TSOD strategy. The overall junction temperature differences are 13.4 °C for TSOD-SFV-PI (blue), 9.7 °C for TSOD-RPI-PI (green) compared to 18.0 °C for PI (gray) in Fig. 22, and are 12.5 °C for TSOD-RPI-FCSMPC (purple) compared to 14.8 °C for FCSMPC (yellow) in Fig. 23. Besides, TSOD-SFV-PI has a stronger response to the upper bound border from 26 min to 30 min and from 52 min to 60 min, where the switching frequency gradually changes, from 8 kHz to 5 kHz and from 9.6 kHz to 6.9 kHz, respectively, as shown in Fig. 19(a), in order to prevent the junction temperature from exceeding the upper bound border 100 °C. The high consistency of the estimated and measured case temperatures in both Fig. 22 and 23 strengthens the accuracy of the online junction temperature estimation and the authenticity of the conclusions derived from the above junction temperatures. Thus, the proposed centralized TSOD strategy has demonstrated its performance on the thermal stress reduction by reducing the swing value of the junction temperature in the experiments.

**TABLE IX Summary and Comparison of PI and FCSMPC Controllers with Centralized Thermal Stressed Oriented Dispatch Strategy**

| Method | Centralized TSOD Strategy | | | Local Controller | Thermal Stress and Reliability Assessment | | | | Other |
|---|---|---|---|---|---|---|---|---|---|
| Name | Dispatch Action | Dispatch Algorithm | Coordination /Communication demands | Additional control scheme | Controlled Loss | Junction Temperature Mean/Swing | Accumulative Damage | Predicted Lifetime | Energy Production/ Efficiency |
| PI | NO | NO | NO | NO | NO | Medium/Medium | High | Low | Medium |
| FCS-MPC | NO | NO | NO | NO | NO | Medium/Medium | Medium | Medium | Medium |
| TSOD-SFV-PI | $f_{sw}$ | SFV, Deterministic, Linear calculation | NO | Modulation scheme | $P^{swit}$ | Low/Low | Low | High | High |
| TSOD-RPI-PI | $Q$ | RPI, Non-deterministic, Nonlinear programming | YES | NO | $P^{cond}$, $P^{swit}$ | High/Low | Medium | Medium | Low |
| TSOD-RPI-FCSMPC | $Q$ | RPI, Non-deterministic, Nonlinear programming | YES | NO | $P^{cond}$, $P^{swit}$ | High/Low | Low | High | Low |

To put everything in a nutshell, the proposed centralized thermal stress oriented dispatch strategy with different dispatch methods, the reliability assessment, and the tradeoff analysis are all summarized in Table IX. A qualitative scale is adopted. The proposed TSOD strategy shows a significant performance on the thermal stress reduction for paralleled grid-connected inverters. Some perspectives of the industry application are evaluated and compared. The switching frequency variation can be decentralized, which eliminates the communication impact from the latency and the error rate. However, the advanced modulation scheme in each local controller is always a concern and asks for more stability testing. The reactive power injection relies on the system communication. But, with the proposed TSOD strategy, the requirement on the transmission speed is low and the latency tolerance is high. Furthermore, the upgrade on the existing industrial drive is minimum by this method. In addition, a strong support on the FCS-MPC is also reflected for future wide industry applications, benefiting from its longer predicted lifetime and the close system efficiency, compared with the conventional PI controller.

## VI. CONCLUSION

In this article, a centralized thermal stress oriented dispatch strategy is proposed to reduce the thermal stresses for paralleled grid-connected inverters. In the proposed strategy, the instantaneous thermal stress is identified first, followed by the expected junction temperature and power loss calculations. Then, the proposed strategy takes full advantage of the local control level methods, including the switching frequency variation and the reactive power injection, to generate the expected power loss and achieve a desired thermal profile with a reduced thermal stress for all paralleled inverters.

The effectiveness of the proposed strategy on the thermal stress reduction is justified through the real-time simulation and the reliability assessment from a four-paralleled-inverters system. Besides, the experiments are also demonstrated on a digital twin hardware platform. Evaluations are attached between different local thermal stress reduction methods, between different local converter controls, and between with and without the proposed TSOD strategy. It turns out that with the proposed TSOD strategy, the thermal stresses are significantly reduced for both PI and FCS-MPC controlled inverters. Considering the tradeoff on the system efficiency, the proposed TSOD strategy with the switching frequency dispatch algorithm will be chosen to achieve the least thermal stress, the longest lifetime, and the highest system efficiency for all paralleled inverters.

## REFERENCES


[1] F. Blaabjerg, R. Teodorescu, M. Liserre, and A. V. Timbus, "Overview of control and Grid synchronization for distributed power generation systems," *IEEE Trans. Ind. Electron.*, vol. 53, no. 5, pp. 1398–1409, Oct. 2006.

[2] K. Ma, M. Liserre, F. Blaabjerg, and T. Kerekes, "Thermal loading and lifetime estimation for power device considering mission profiles in wind power converter," *IEEE Trans. Power Electron.*, vol. 30, no. 2, pp. 590–602, Feb. 2015.

[3] A. S. Bahman, K. Ma, P. Ghimire, F. Iannuzzo, and F. Blaabjerg, "A 3-D-Lumped thermal network model for long-term load profiles analysis in high-power IGBT modules," *IEEE J. Emerg. Sel. Top. Power Electron.*, vol. 4, no. 3, pp. 1050–1063, Sep. 2016.

[4] D. Zhou, H. Wang, and F. Blaabjerg, "Mission profile based system-level reliability analysis of DC/DC converters for a backup power application," *IEEE Trans. Power Electron.*, vol. 33, no. 9, pp. 8030–8039, Sep. 2018.

[5] A. Sangwongwanich, Y. Yang, D. Sera, and F. Blaabjerg, "Mission profile-oriented control for reliability and lifetime of photovoltaic inverters," *IEEE Trans. Ind. Appl.*, vol. 56, no. 1, pp. 601–610, Jan./Feb. 2020.

[6] R. Bayerer, T. Herrmann, T. Licht, J. Lutz, and M. Feller, "Model for power cycling lifetime of IGBT modules - various factors influencing lifetime," in *Proc. 5th Int. Conf. Integr. Power Electron. Syst.*, Nuremberg, Germany, 2008, pp. 1–6.

[7] M. Andresen, K. Ma, G. Buticchi, J. Falck, F. Blaabjerg, and M. Liserre, "Junction temperature control for more reliable power electronics," *IEEE Trans. Power Electron.*, vol. 33, no. 1, pp. 765–776, Jan. 2018.

[8] D. A. Murdock, J. E. R. Torres, J. J. Connors, and R. D. Lorenz, "Active thermal control of power electronic modules," *IEEE Trans. Ind. Appl.*, vol. 42, no. 2, pp. 552–558, Mar./Apr. 2006.

[9] T. A. Polom, B. Wang and R. D. Lorenz, "Control of junction temperature and its rate of change at thermal boundaries via precise loss manipulation," *IEEE Trans. Ind. Appl.*, vol. 53, no. 5, pp. 4796–4806, Sep./Oct. 2017.

[10] L. Wei, J. McGuire, and R. A. Lukaszewski, "Analysis of PWM frequency control to improve the lifetime of PWM inverter," *IEEE Trans. Ind. Appl.*, vol. 47, no. 2, pp. 922–929, Mar./Apr. 2011.

[11] Y. Ko, M. Andresen, G. Buticchi, and M. Liserre, "Thermally compensated discontinuous modulation strategy for cascaded H-Bridge converters," *IEEE Trans. Power Electron.*, vol. 33, no. 3, pp. 2704–2713, Mar. 2018.

[12] Y. Ko, M. Andresen, G. Buticchi, and M. Liserre, "Discontinuous modulation based active thermal control of power electronic modules in wind farms," *IEEE Trans. Power Electron.*, vol. 34, no. 1, pp. 301–310, Jan. 2019.

[13] J. Lemmens, J. Driesen and P. Vanassche, "Dynamic DC-link voltage adaptation for thermal management of traction drives," in *Proc. IEEE Energy Convers. Congr. Expo.*, Denver, CO, USA, 2013, pp. 180–187.

[14] J. Lemmens, P. Vanassche, and J. Driesen, "Optimal control of traction motor drives under electrothermal constraints," *IEEE J. Emerg. Sel. Top. Power Electron.*, vol. 2, no. 2, pp. 249–263, Jun. 2014.

[15] K. Ma, M. Liserre, and F. Blaabjerg, "Reactive power influence on the thermal cycling of multi-MW wind power inverter," *IEEE Trans. Ind. Appl.*, vol. 49, no. 2, pp. 922–930, Mar./Apr. 2013.
[16] Y. Yang, H. Wang, and F. Blaabjerg, "Reactive power injection strategies for single-phase photovoltaic systems considering grid requirements," *IEEE Trans. Ind. Appl.*, vol. 50, no. 6, pp. 4065–4076, Nov./Dec. 2014.
[17] D. Zhou, F. Blaabjerg, M. Lau, and M. Tonnes, "Thermal behavior optimization in multi-MW wind power converter by reactive power circulation," *IEEE Trans. Ind. Appl.*, vol. 50, no. 1, pp. 433–440, Jan./Feb. 2014.
[18] D. Zhou, F. Blaabjerg, M. Lau, and M. Tønnes, "Optimized reactive power flow of DFIG power converters for better reliability performance considering grid codes," *IEEE Trans. Ind. Electron.*, vol. 62, no. 3, pp. 1552–1562, Mar. 2015.
[19] J. Falck, G. Buticchi, and M. Liserre, "Thermal stress based model predictive control of electric drives," *IEEE Trans. Ind. Appl.*, vol. 54, no. 2, pp. 1513–1522, Mar./Apr. 2018.
[20] L. Wang, J. He, T. Han, and T. Zhao, "Finite control set model predictive control with secondary problem formulation for power loss and thermal stress reductions," *IEEE Trans. Ind. Appl.*, vol. 56, no. 4, pp. 4028–4039, Jul./Aug. 2020.
[21] L. Wang, T. Zhao, and J. He, "Investigation of variable switching frequency in finite control set model predictive control on grid-connected inverters," to be published.
[22] S. Kouro, P. Cortes, R. Vargas, U. Ammann, and J. Rodriguez, "Model predictive control—A simple and powerful method to control power converters," *IEEE Trans. Ind. Electron.*, vol. 56, no. 6, pp. 1826–1838, Jun. 2009.
[23] J. Rodriguez *et al.*, "State of the Art of finite control set model predictive control in power electronics," *IEEE Trans. Ind. Informat.*, vol. 9, no. 2, pp. 1003–1016, May 2013.
[24] S. Vazquez *et al.*, "Model predictive control: A review of its applications in power electronics," *IEEE Ind. Electron Mag.*, vol. 8, no. 1, pp. 16–31, Mar. 2014.
[25] S. Kouro, M. A. Perez, J. Rodriguez, A. M. Llor, and H. A. Young, "Model predictive control: MPC's role in the evolution of power electronics," *IEEE Ind. Electron. Mag.*, vol. 9, no. 4, pp. 8–21, Dec. 2015.
[26] S. Vazquez, J. Rodriguez, M. Rivera, L. G. Franquelo, and M. Norambuena, "Model predictive control for power converters and drives: Advances and trends," *IEEE Trans. Ind. Electron.*, vol. 64, no. 2, pp. 935–947, Feb. 2017.
[27] P. Karamanakos, E. Liegmann, T. Geyer, and R. Kennel, "Model predictive control of power electronic systems: Methods, results, and challenges," *IEEE Open J. Ind. Appl.*, vol. 1, pp. 95–114, Aug. 2020.
[28] V. S. Neary *et al.*, "Methodology for design and economic analysis of marine energy conversion (MEC) technologies," USA, 2014. [Online]. Available: https://energy.sandia.gov/wp-content/gallery/uploads/SAND2014-9040-RMP-REPORT.pdf
[29] R. Bayerer, T. Herrmann, T. Licht, J. Lutz, and M. Feller, "Model for power cycling lifetime of IGBT modules - various factors influencing lifetime," in *Proc. 5th Int. Conf. Integr. Power Electron. Syst.*, 2008, pp. 1–6.
[30] M.A. Miner, "Cumulative damage in fatigue," *J. Appl. Mech.*, vol. 12, pp. A159–A164, 1945.
[31] E. O¨ zkol, S. Hartmann, and H. Duran, "Load-cycling capability of HiPak IGBT modules ABB Application Note 5SYA 2043-04," Jan. 2012. [Online]. Available: https://library.e.abb.com/public/1f4fb71e0af3356883257c8d00443ca1/Load-cycling%20capability%20of%20HiPak_5SYA%202043-04.pdf
[32] ABB ACS 800-17. Line-side Converter 120 to 1385 kVA User's Manual, 2013. [Online]. Available: https://library.e.abb.com/public/af11323bb0ed51c2c1256d5a0057f03d/en_aca635_um_and_update_D.pdf
[33] ABB HiPak 5SND0800M170100 IGBT Module, 2014. [Online]. Available: https://new.abb.com/products/5SND0800M170100/dual-hipak-igbt-module
[34] Moored Acoustic Doppler Current Profiles in Gulf Stream, Florida, FL, USA. 2014. [Online]. Available: http://coet.fau.edu/resource-measurement-modeling/available-data.html
[35] H. Niu and R. D. Lorenz, "Evaluating different implementations of online junction temperature sensing for switching power semiconductors," *IEEE Trans. Ind. Appl.*, vol. 53, no. 1, pp. 391–401, Jan./Feb. 2017.
[36] Infineon IKCM15L60GD Intelligent Power Module, 2016. [Online]. Available: https://www.infineon.com/cms/en/product/power/intelligent-power-modules-ipm/ikcm15l60gd/

**LUOCHENG WANG** (Student Member, IEEE) received the B.S. degree in electrical engineering from the University of Connecticut, Storrs, CT, USA, in 2014, and the M.Eng. degree in electrical and computer engineering from Cornell University, Ithaca, NY, USA, in 2016. He is currently working toward the Ph.D. degree in electrical and computer engineering with the University of North Carolina at Charlotte, Charlotte, NC, USA. His current research interests include advanced control of power converters and electrical drives, model predictive control, reliability in power electronics, grid-integration of renewable energy systems and inductive power transfer.

**TIEFU ZHAO** (Senior Member, IEEE) received the B.S. and M.S. degrees from Tsinghua University, Beijing, China, in 2003 and 2005, respectively, and the Ph.D. degree from North Carolina State University, Raleigh, in 2010, all in electrical engineering.

From 2010 to 2016, he was with Eaton Corporation Research & Technology, Milwaukee, WI. Since 2016, he has been an Assistant Professor of Electrical and Computer Engineering and an Associate of the Energy Production and Infrastructure Center (EPIC) with the University of North Carolina at Charlotte, Charlotte, NC, USA. He has authored or coauthored more than 40 papers in refereed journals and international conference proceedings. He has 12 patents awarded. His current research interests include solid state transformer and solid state circuit protection, wireless power transfer, microgrid and renewable energy integration, wide bandgap device applications, and power electronics reliability.

Dr. Zhao was the recipient of 2015 IAS Andrew W. Smith Outstanding Young Member Award and 2015 STEM Forward Young Engineer of the Year Award. Dr. Zhao was an Associate Editor for the IEEE JOURNAL OF EMERGING AND SELECTED TOPICS IN POWER ELECTRONICS (JESTPE). He was the Organizing Committee Member on several international conferences, including ECCE 2016-2019 and PEDG 2018. He is the Founding Chair of IEEE Charlotte section PELS/IAS/IES Chapter.

**JIANGBIAO HE** (Senior Member, IEEE) received the Ph.D. degree in electrical engineering with an emphasis on power energy conversion from Marquette University, Milwaukee, WI, USA. He is currently an Assistant Professor with the Department of Electrical and Computer Engineering, the University of Kentucky, USA. He previously worked in industry, most recently as a Lead Engineer with GE Global Research, Niskayuna, New York, NY, USA. He also worked with Rockwell Automation and Eaton Corporate Research before he joined GE in 2015. His research interests include transportation electrification, renewable energy, and fault-tolerant operation of power conversion systems for safety-critical applications.